Proceedings World Geothermal Congress 2020+1
Reykjavik, Iceland, April - October 2021

Characteristic of Pore Pressure Migration Clarified by Multidisciplinary Microseismic Analysis

Yusuke Mukuhira, Takatoshi Ito, Hirokazu Moriya, Hiroshi Asanuma, Markus Häring

Institute of Fluid Science, Tohoku University, 2-1-1 Katahira, Aoba-ku, Sendai, 980-8577, Japan

mukuhira@tohoku.ac.jp

Keywords: EGS, microseismicity, pore pressure, in-situ stress, stimulation, shut-in, fluid flow, Basel

ABSTRACT

Understanding the pore pressure migration during the hydraulic stimulation is an essential factor to realize the Engineered Geothermal System (EGS) type development. It is beneficial for mitigating the risk of unexpected of large induced seismicity and enhancing the sustainability of the reservoir. The fluid flow occurred due to the injection can be tracked by monitoring microseismicity. The standard microseismic analysis provides information that pore pressure increases to some level. But microseismic information does not provide quantitative information about pore pressure. We fully utilized the in-situ stress information of stress magnitude and orientation, and geometry of existing fractures estimated by microseismic analysis. Then, we inverted the pore pressure increase required to generate shear slip on an existing fracture during stimulation. Spatiotemporal analysis of estimated pore pressure increase provided a lot of critical observations about pore pressure migration during and after the stimulation. We observed the pore pressure redistribution at the shut-in phase, and pore pressure gradient from injection point disappeared, causing the pore pressure distribution nearly uniform. We interpreted that the higher pore pressure near the injection well migrated to the far-field. The redistribution of the pore pressure caused the large induced seismicity, which often occurred significantly at the edge of the previously stimulated zone. Another observation from the spatiotemporal distribution of pore pressure is that lower pore pressure migrates farther and faster. Meanwhile, higher pore pressure migrates more slowly. We were able to interpret these phenomena successfully with the relationship between fracture permeability and state of stress. Existing fracture in critical condition is more permeable than those in less critical condition. So, low pore pressure migrates via permeable and critical fractures causing the seismicity. Then, permeabilities of those fractures are enhanced furthermore, promoting farther migration of low pore pressure. When wellhead pressure reached a certain point, the migration characteristic has changed. The higher pore pressure stagnated near the injection point started migrating to the far-field, which decreased the higher migration rate of lower pore pressure. From these observations, we interpret that there is the most productive wellhead pressure, which promotes the migration of low pore pressure in a broader region according to each EGS reservoir characteristics.

1. INTRODUCTION

Hydraulic stimulation is an essential technology for enhancing the permeability of the target reservoir for Enhanced/Engineered Geothermal System (EGS) projects. Many EGS projects deployed hydraulic stimulation to create an artificial geothermal reservoir. Hydraulic stimulation is extending its application from geothermal to unconventional resources development such as shale gas and oil in the form of hydraulic fracturing. Associated with the expansion of the use of fluid injection operation, the occurrence of the unexpected size of induced seismicity has become the serious environmental issues (Majer et al., 2007; Suckale, 2009; Evans et al., 2012; Ellsworth, 2013). However, fluid injection is the necessary technology for geothermal future, and microseismicity originated from the shear slip is also a part of microseismic monitoring. Therefore, regulations and strategy to mitigate the risk of induced seismicity have been requested by the industry and the public. To develop those risk assessment technology, having a better understanding of the physics of the large events is essential as well as the understanding of the behavior of the pore pressure migration

With the increasing EGS projects in the last two decades, it has been cleared that one of the characteristics of the large induced seismicity from the geothermal field. One of them is that the large induced seismicity tends to occur after the stop of injection, i.e., shut-in phase (Majer et al., 2007). Injection-induced seismicity is caused by the simply increased pore pressure, even though the other physical parameters such as Coulomb stress changes (Catalli et al., 2013), thermal stress (Ghassemi and Zhou, 2011), and poroelastic stress (Segall and Lu, 2015) have a potential to trigger the shear slip. Especially for the induced seismicity occurred just after shut-in, we can reasonably assume that re-distribution of pore pressure according to the stop of the injection. So, we utilized the microseismic data from Basel, Switzerland EGS project where ML 3.4 event occurred just after the shut-in to investigate the mechanisms of shut-in event. We also used the in-situ stress data measured throughout borehole logging, and then we managed to estimate pore pressure from the microseismic-geomechanical analysis. Finally, we investigated the pore pressure migration behavior during and after shut-in, also found the causality of pore pressure migration behavior to the occurrence of large induced events. This paper is summarizing work of our previous articles (Mukuhira et al., 2016; Mukuhira et al., 2017).

2. FIELD OUTLINE

2.1 Hydraulic stimulation

The injection well of Basel-1 was drilled into the granitic basement rock lying under 2.4 km of sedimentary rocks in the urban area of Basel. The total depth of Basel-1 was 5000 m from the ground surface, and the lower part from 4629 to 5000 m was an open hole section (Häring et al., 2008). The open hole section of Basel-1 was subjected to hydraulic stimulation that injected around 11,500 m^3 of freshwater through several permeable zones (Häring et al., 2008). Wellhead pressure reached 29.6 MPa at 3300 L/min flow on 8th December, after the sixth day of the start of hydraulic stimulation. The first felt event with M_L 2.6 occurred early of the same day, exceeding the magnitude criterion on a traffic light system employed for this field. According to the protocol, the flow rate was

reduced, then injection was stopped by shutting-in the wellhead. Despite these effort to shut down the stimulation safely, the largest event of M_L 3.4 occurred just after the shut-in (Figure. 1). This event required bleeding off since well shut-in was not successful in suppressing seismic activity (Häring et al., 2008). The M_L 3.4 event caused widely felt shaking and some damage to local buildings in Basel (Giardini, 2009). Seismic activity decreased significantly after bleeding off; however, several large events with ML >3.0 were still recorded in mid-2007 (Mukuhira et al., 2013).

2.2. Monitoring Network

The microseismic activity was monitored by the operating company, Geothermal Explorer Ltd. (GEL; currently Geo Explorer Ltd.). They installed the local microseismic network consisted of six downhole seismometers of three components and one temporary seismometer in an injection well. This microseismic network and well constrained velocity model enabled to determine the precise hypocenter location (Dyer et al., 2008; Häring et al., 2008). Microseismic network captured approximately 13,000 seismic events during and after stimulation with the trigger system, and GEL determined the hypocenters for around 2700 events in nearly real-time by February 2007 (Asanuma et al., 2007). The Swiss Seismological Service (SED) also monitored seismic activity using their monitoring network for natural earthquakes in Switzerland (Deichmann et al., 2014). SED network detected several induced events with relevant magnitude, and they determined the fault plane solutions (FPSs) of induced seismicity large enough to be detected.

2.3. Microseismic Data

Our previous study determined the hypocenter locations of microseismic events using conventional hypocenter determination method, after manual picking in near real-time (Asanuma et al., 2007). Based on these absolute locations, we applied multiplet analysis (i.e., cluster analysis) referring waveform similarity (Moriya et al., 2003), and relocated the precise hypocenter location (Asanuma et al., 2008) with the double-difference method (Waldhauser and Ellsworth, 2000). We found multiplet clusters represent sub-vertical linear or planar structures. Their strikes are aligned to the direction of ± 30° from the orientation of the maximum regional horizontal stress (N144°E±14°). This study is based on the result of relocation from Asanuma et al. (2008). The hypocenter locations of induced seismicity we used in this study are shown in Figure 2. The microseismic distribution delineated a sub-vertical macroscopic seismic structure oriented approximately NNW–SSE, consistent with the regional stress state.

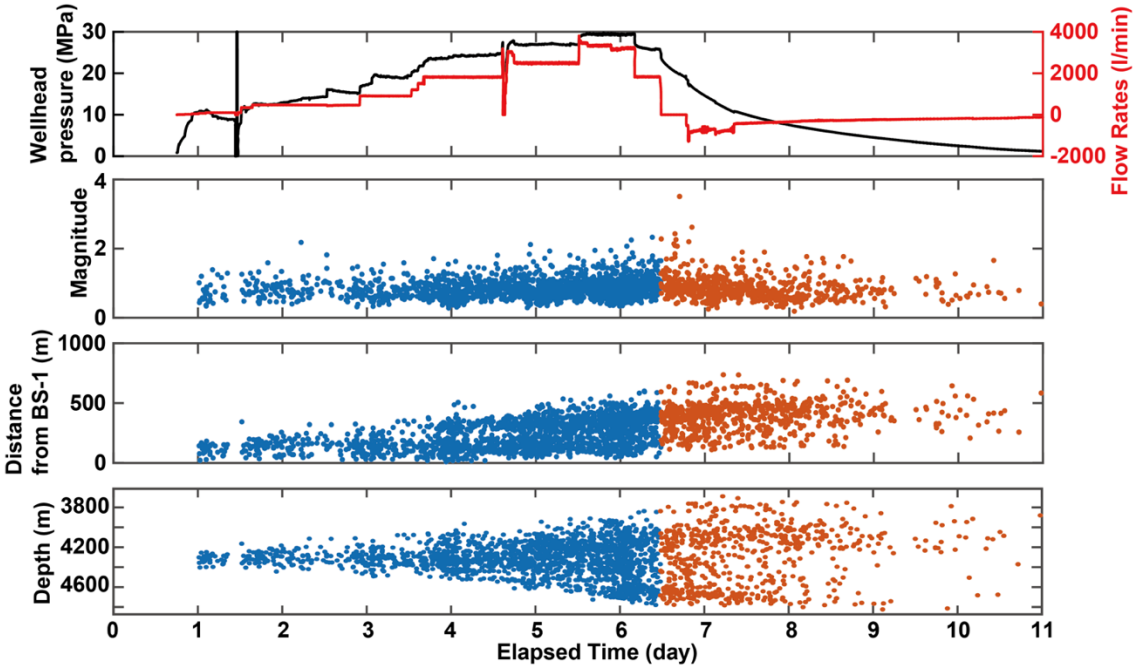

Figure 1. (Top) Profile of wellhead pressure (black line) and injection flow rate (red line) of hydraulic stimulation at Basel from the start (2 December) to 13 December. Shut-in time is 11:33 on 8 December, where the color of microseismic events changes in other panels. (2nd) Time history of moment magnitude (Mw) of induced seismicity recorded by microseismic monitoring network. (3rd) One dimensional distribution of event distance from the injection point. (4th) One dimensional depth migration from the main injection point.

2.5. Characteristics of Shut-in Events

First, we summarized the characteristics of microseismic events before and after shut-in. We split the seismic catalog at the time of shut-in 11:33 local time on 8 December and the results of a simple time series analysis are shown in Figure 1. The larger events significantly occurred in the next 12 h after shut-in (Figure 1). In total, the 14 large events with M_w>2.0 occurred by the 11th day of the stimulation, but 9 of the events, including the largest event, occurred after shut-in. The 3rd panel of Figure 1 shows the distance of each seismic event from the estimated main feed point. The figure is an r-t plot of diffusion models (e.g., Shapiro and Dinske, 2009) and provides an overview of microseismic cloud progression in one dimension. The microseismic distribution fitted well with a trigger front for diffusivity of 0.05 m^2/s (Dinske et al., 2010). The seismic cloud had extended over the study period. This observation suggests that pore pressure migration continued in this time period even after the stop of injection. From the vertical hypocenter migration in the 4th panel of Figure1, the microseismic zone tended to progress toward the deep and shallow parts of the reservoir, although active seismic activity was much more frequently observed in the shallow rather than deep part of the reservoir. Figure 2

shows the 3-dimensional contrast of hypocenter distribution before/after shut-in. The microseismic events after shut-in occurred from the periphery of the seismic cloud, and microseismic activity at shut-in phase considerably pushed the seismic front of the seismic cloud.

In contrast, few events occurred in the previously seismically active zone, where thousands of seismic events had occurred during stimulation. We also found that several larger events (M_w>2.0) occurred at the edge of the seismic cloud (Figure 2). These observations strongly suggest causality between the occurrence of large events and shut-in. More of the large events were observed in the deeper part of the reservoir and also in the shallow part, although the deeper part showed more seismic activity, as shown in Figure 2. These fundamental observations were the starting point of this study. We estimated pore pressure using microseismic data and regional stress information and then investigated the behavior of shut-in pressure, i.e., how pore pressure propagated at the shut-in phase. The causality of the occurrence of large induced seismicity after shut-in was investigated to clarify the physical mechanism governing the large magnitude seismicity.

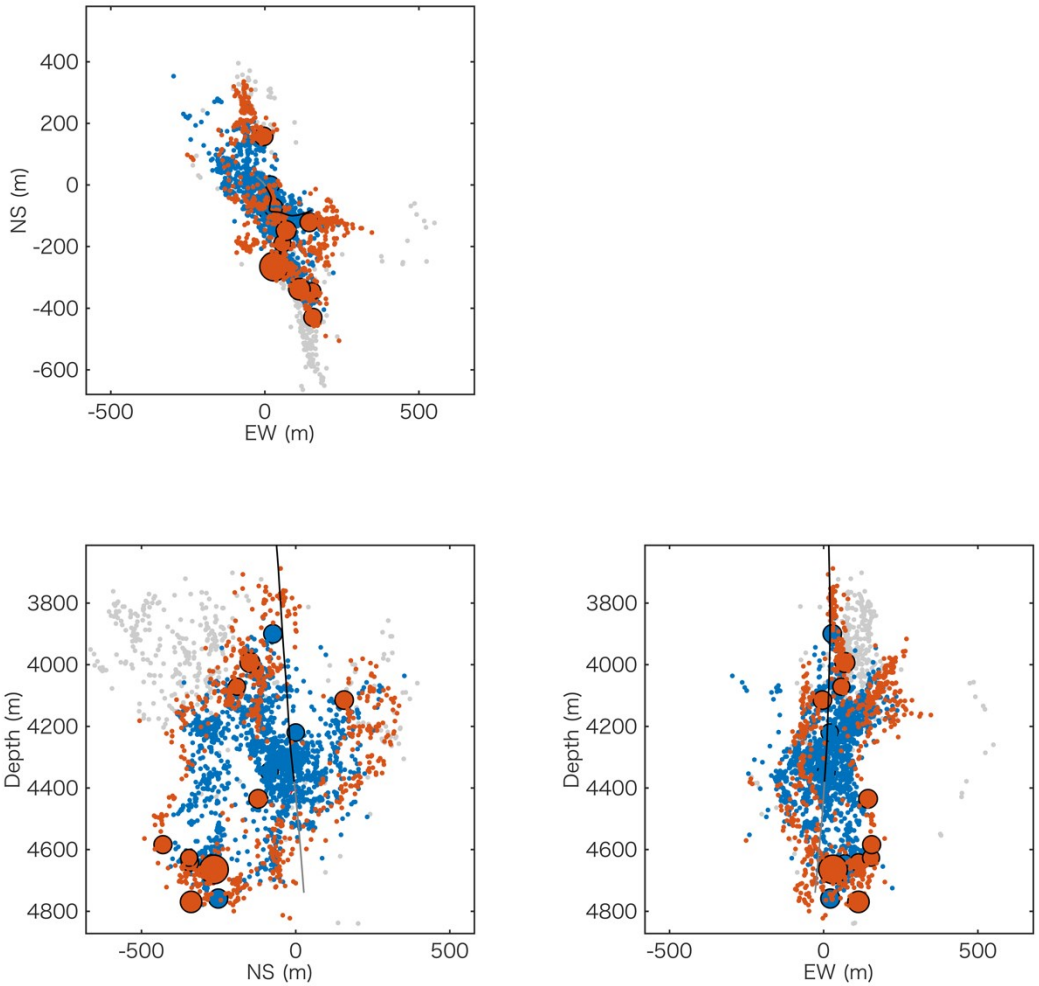

Figure 2. Hypocenter distribution of microseismic events at Basel EGS project. Color of plots correlates event's occurrence time as Figure 1. Blue dots show the events that occurred during the stimulation, and Red dots show the events that occurred after the shut-in. Grey dots indicate the events that occurred after the study period shown in Figure 1. The black line indicates injection well of Basel-1 and gray parts is open hole section. In this scale, depth is from sea level.

3. METHODOLOGY

3.1 Methodology

When stress orientation and stress magnitude, and geometry of fault plane are available, shear and normal stress working on a given fault plane can be computed with geomechanical theory. Then, the friction coefficient is given, necessary pore pressure increase to have shear slip is estimated by the Coulomb failure criterion:

$$\tau = \mu(\sigma_n - P_h - P_c) \tag{1}$$

where τ is shear stress, μ is friction coefficient, σ_n is normal stress, and P_c is pore pressure increase to have a shear slip.

In the process of pore pressure estimation, we assumed homogeneous stress state in the reservoir in time and space, and we modeled stress state of this field with the stress model of Valley and Evans (2015) as a function of depth. We did not consider the heterogeneity of elastic property for simplicity. As second assumptions, we used a constant friction coefficient of 0.6 (Byerlee, 1978) for all fault planes. In this analysis, we considered that all induced seismicity was triggered only by an increase of pore pressure, and did not

consider contributions of other parameters e.g., Coulomb stress change by preceding events, nucleation of thermal stress caused by cold water injection, and chemical effect on friction coefficient for the reason we stated before.

3.2 *In-situ* stress information

Valley and Evans (2006, 2009) analyzed the orientation of breakouts and drilling-induced tensile fractures in the injection well (Basel-1) and the deepest monitoring well (OT-2). They reported that orientation of the maximum horizontal stress (S_{HMax}), within the granite section at Basel is N144◦E±14◦. Their estimation is consistent with the focal mechanism of natural earthquakes in this region, and larger events occurred by hydraulic stimulation. The magnitude of vertical stress (S_v) was estimated from density logs, and the magnitude of horizontal stress was estimated from core samples (Häring et al., 2008). Valley and Evans (2015) reported stress magnitude inferred from borehole breakout width analysis. In summary, we used the stress model given by equation (2) ~ (5). According to the updated stress state, S_{Hmax} can be modeled as a small gradient function of depth. The stress state transits strike slip to normal faulting at around 4800 m depth because differential stress decreases with depth and S_v becomes larger than S_{Hmax} at that depth.

$$S_{HMmax} = 0.00104z + 115 \tag{2}$$

$$S_{hmin} = 0.01990z - 17.78 \tag{3}$$

$$S_v = 0.0249z \tag{4}$$

$$P_h = 0.00981z \tag{5}$$

where S_{Hmax} is maximum horizontal stress, S_{hmin} is maximum horizontal stress, S_v is vertical stress, P_h is hydrostatic pressure, and z is depth respectively. Units for all parameters here are MPa except z is in meter.

3.3 Fault geometry

Fault plane solutions (FPSs) for 28 larger events were estimated by Deichmann and Giardini (2009), using polarity information of first motion from SED monitoring network as well as the microseismic network of GEL. Many of FPSs showed strike slip type focal mechanism. Terakawa et al. (2012) showed more FPSs for a total of 118 events which were provided from SED. We used this FPS information for larger events. It should be noted that the selection of actually slipped fault plane from two nodal planes of FPSs. We first checked the pore pressure increase for both nodal planes. If pore pressure increase of one from both nodal planes is more than maximum wellhead pressure which was a physical limit, we simply choose the one of smaller pore pressure. If pore pressure increase of both nodal planes were less than maximum wellhead pressure, we compared three-dimensional geometries of both nodal planes and hypocenter distribution of periphery events for every single larger event. Then one having harmonious geometry with neighboring events was chosen.

For many of other events which their fault mechanisms were not estimated due to their small magnitude, we used the result of multiplet analysis. Many of the multiplet cluster in this field showed ellipsoidal or streak geometry (Asanuma et al., 2008). So, we estimated the geometry of multiplet cluster from hypocenter distribution of multiplet events and used as the orientation of fault plane under the assumption that multiplet event in the same cluster occurred from the same existing fracture. Reliability of fault plane orientation of multiplet events was lower than the fault mechanism of SED.

3. RESULTS

3.1 Pore pressure migration during the stimulation

Figure 3 shows the one-dimensional pore pressure nucleation in the relationship between the distance from the estimated injection point in the injection well and pore pressure increase. Each snapshot was taken every 0.5 days. All the pore pressure data up until each time step, are shown in Figure 1, and those pore pressure should remain until the reduction of the injection or significant increase in permeability. The wellhead pressure at each time step is also shown with stars on a distance zero that means injection point. The values of pore pressure shown as dots within circles were estimated from the FPSs of SED, and the values illustrated by only dots were obtained from cluster analysis. The pore pressure estimates based on the FPSs are much more robust and have higher reliability. Since wellhead pressure should be the highest in the system and pressure source of the stimulation, pore pressure estimates higher than the wellhead pressure should be artifacts.

We observed that lower pore pressure migrated faster and farther throughout the entire stimulation period, which was particularly evident between day 2.5 and 5. From Figure 3, the extent of the seismically activated zone at each time step can be observed. Pore pressure in the near field of injection well was able to increase to almost the same level as the wellhead pressure. Concurrently, lower pore pressure progressed to about 400 m from the injection point, which was around twice as far as pore pressure more than 10 MPa. This suggests the speed (migration rate) of lower pore pressure (400/4 = 100 m/d) was only twice that of moderate pore pressure (200/4 = 50 m/d).

After 4.5 days, pore pressure > 10 MPa started to migrate farther. Pore pressure exceeding 10 MPa reached the area of 500 m away from the injection well. Similarly, higher pore pressure (>20 MPa) reached a distance of 350 m, progressing 150 m during the same two day period. At the same time, we also observed that the migration rate of lower pore pressure decreased in comparison with the rapid increases of the migration rates of moderate and higher pore pressure after day four besides the higher wellhead pressure. This resulted in a convex shape of the function of the pore pressure-distance curve, even though it was concave before day 4.

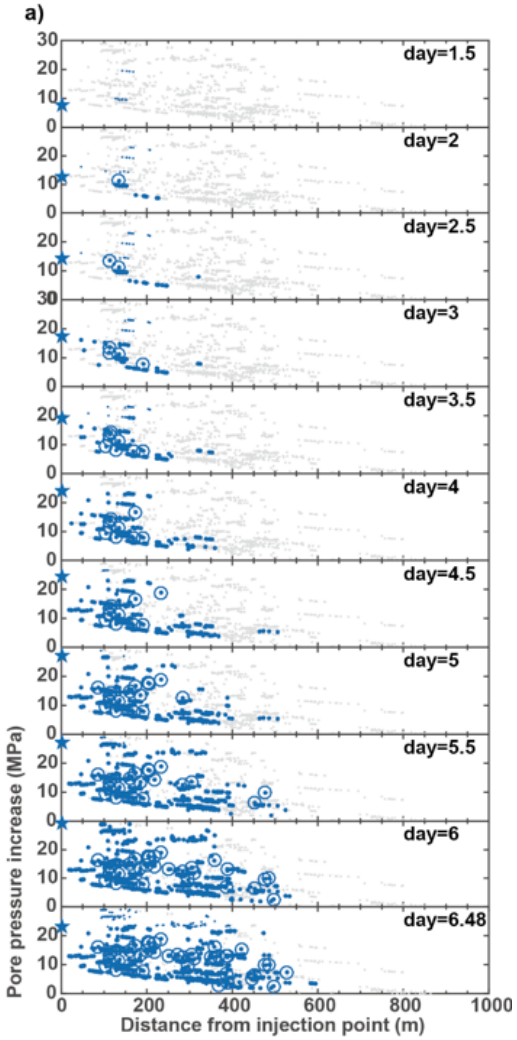

Figure 3. Snapshots of one-dimensional pore pressure distribution to distance from the injection point. Circles with dots show the pore pressure increase estimates based on FPSs from SED. Dots do those based on multiplet analysis. The stars indicate the WHP at each time step. All pore pressure data based on the events that occurred before the time-step is shown in each panel.

3.2 Pore pressure migration at shut-in phase

Figure 4 shows the cross-sectional view of the reservoir with pore pressure estimates before and after the shut-in. The estimates of pore pressure are shown on the hypocenter location of microseismicity. The color of the plots indicates the magnitude of pore pressure. Color code scheme is from blue (0 MPa) to maximum WHP (30 MPa). All pore pressure information before the shut-in is shown in the left panel and same for those after shut-in in the right panel. The black line is the injection well trajectory, and color change from black to gray shows the end of casing zone.

We observed that the seismic cloud is formed from the injection point to outward. Some of the events were triggered by high pore pressure in the vicinity of the injection point. At the edge of the seismic cloud, most of the events occurred under lower or moderate pore pressure increase. Drastically change occurred at the shut-in. The microseismic distribution significantly changed after the shut-in. Microseismic events occurred at the edge of the seismic zone, and seismic activity near the injection well became silence significantly. The colors of the plot for after shut-in indicate that pore pressure remained significantly high enough to cause further microseismicity. Especially in the deep part and shallow part of the reservoir, we can observe the concentration of microseismicity and various pore pressure migration, as we can observe the square marker distributed on the periphery of the seismic cloud. The larger events, including the largest one from the deep part, occurred under a moderate pore pressure (in this case, around 15 MPa) that they are shown with colored squares. The seismic cloud extended to both the deep and the shallow parts of the reservoir rather than a lateral or homogeneous extension of the stimulated zone.

Those observations can also be confirmed in the one-dimensional distribution of pore pressure in Figure 5. Again, Figure 5 shows the relationship between distance from injection point and pore pressure. We can observe that the pore pressure migration at the shut-in phase pushed the trigger front horizon much further. In addition to the distance, the value of pore pressure increased at the boundary of the previously stimulated zone (around 400~600 m in Figure 5). Furthermore, the pressure gradient that we can observe for during stimulation disappeared, and considerable pore pressure (20~25 MPa) distributed homogeneously in the region of 400~550 m from the injection point.

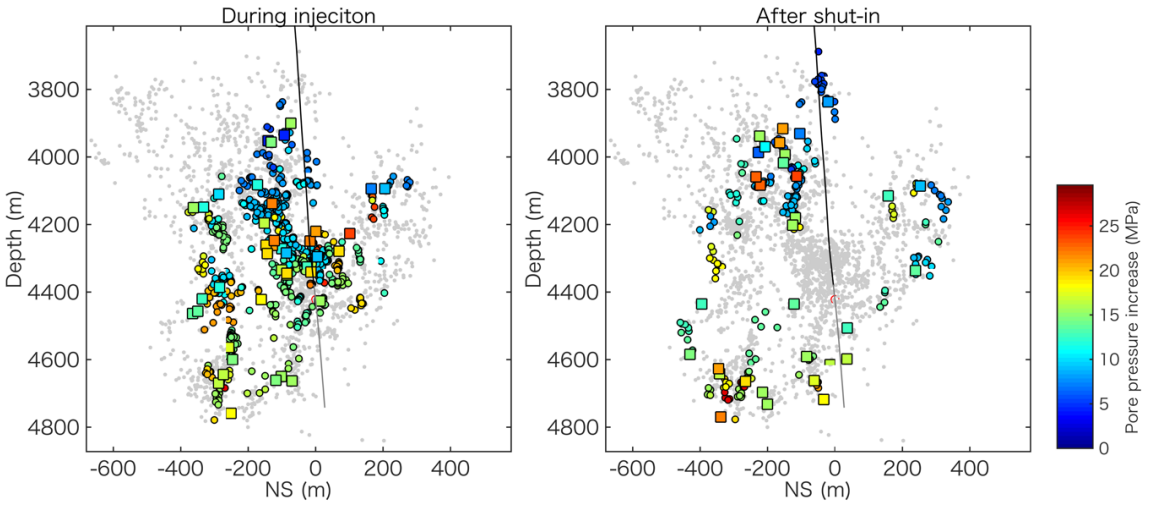

Figure 4: Pore pressure distribution on hypocenter distribution before and after shut-in. Squares correlate the events which their pore pressure increase was estimated from FPSs and dots were those determined from multiplet analysis. Color corresponds pore pressure increase scaled from 0 to maximum wellhead pressure (29.6 MPa). The figure shows the NS cross-section of the reservoir. Grey dots are the other events not associated with this analysis.

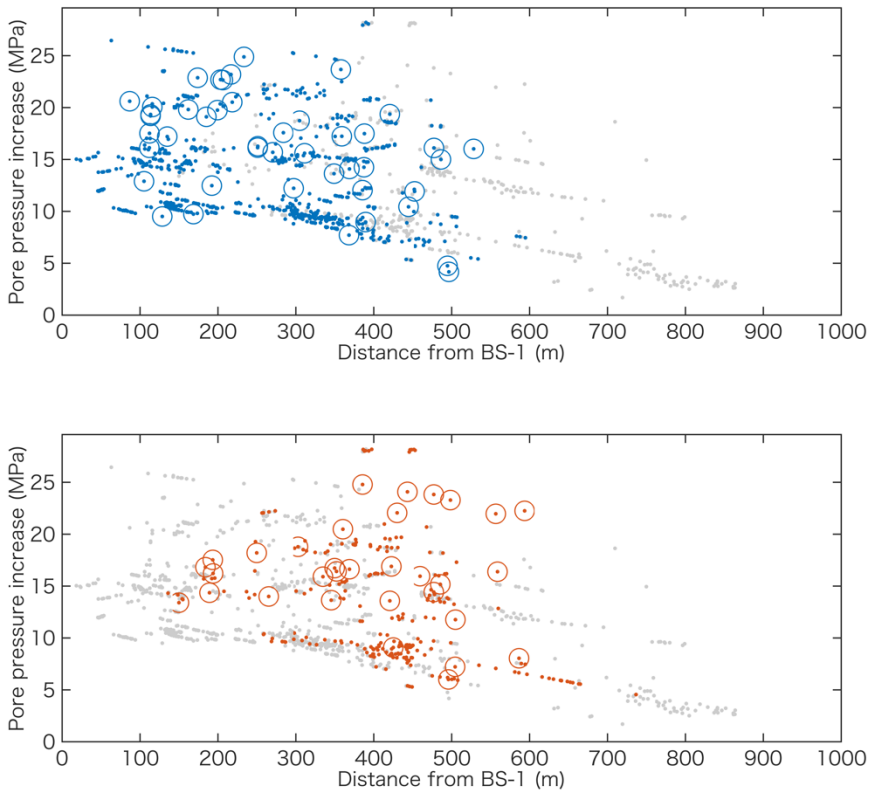

Figure 1: One dimensional pore pressure distribution on hypocenter distribution before (top) and after shut-in (bottom). The figure is the same format to Figure 3. The reference point is the estimated feed point in injection well Basel-1. Grey dots in the background are the events not associated with this analysis.

4. DISCUSSION

4.1 Causality to the LMEs

As we observed, pore pressure propagated further even after shut-in. The increase in pore pressure at the shut-in phase was high enough (in this case ~20 MPa) to trigger shear slip on faults located at the periphery of the previously stimulated region. Therefore, pore pressure migration at the shut-in phase brought significant pore pressure increase in the entire region of the boundary of the stimulated area. During the stimulation, pore pressure decreased with distance from the pressure source, but after shut-in, pore pressure gradient disappeared or weakened. Moreover, pore pressure distributed uniformly in the periphery of the stimulated zone. From these observations, we interpreted that pore pressure migration at the boundary of the stimulated zone was originated by redistribution of pore pressure at the shut-in phase. The higher pore pressure in the vicinity of the injection well during stimulation redistributed to far-field part of the reservoir through the flow path system within the stimulated area (Figure 2). We also interpreted that pore pressure migration stagnated at the edge of the stimulated area due to the contrast of the permeability, that is the boundary of the stimulated and unstimulated area.

Uniformly distributed pore pressure at the peripherical area of the stimulated zone after shut-in caused most of the larger existing fault a critical state, and this caused the shear slip of entire fault resulting in the outbreak of large induced seismicity. Therefore, we consider the migration of pore pressure is the dominant driving cause to lead the occurrence of the large induced seismicity. We further interpreted that pore pressure is not necessary to be the reason to cause the broader area of fault in critical condition. Any physical phenomena in the reservoir can create this situation, but pore pressure is the leading driving cause for the shut-in case.

4.2 Pore pressure migration process

We observed that the migration rate of pore pressure is dependent on pore pressure and that lower pore pressure tends to advance farther and faster. As we estimate pore pressure increase geomechanically, the lower pore pressure means that the fault planes oriented favorably to the stress state, i.e., a subcritical state. Meanwhile, it has been revealed that critically stressed faults are the most permeable faults and the permeability of the fault is dependent on its stress state (e.g., Barton et al., 1995; Ito and Zoback, 2000). Therefore, a subcritical fracture which can be caused by lower pore pressure increase may have higher permeability. On the contrary, the fault planes that require higher/moderate ΔPs for shear slip correspond to fractures not oriented favorably, and thus, the permeability of such fractures would be lower than those oriented favorably. This is precisely the reason why lower pore pressure advances farther and faster and why higher/moderate pore pressure migrates outward slowly. We interpreted that injected fluid intrudes selectively into permeable fractures. Then, these fractures cause shear slip and enhance their permeability further. This process continues repeatedly, and it would promote the progress of the seismic zone activated by lower pore pressure, as long as a sufficient volume of fluid was supplied to maintain pore pressure. This process would be a "self-migrating mechanism." It should be noted that higher pore pressure started migration only after wellhead pressure reached 20 MPa, which could cause a certain delay, especially for higher ΔP. However, the reason behind the significant migration of higher/moderate ΔP, observed after day 4 in the current study, remains an open question.

The migration rate of lower pore pressure decreased after the start of the progress of higher/moderate pore pressure. The lower pore pressure advanced only around 200 m during days 4–6 despite the wellhead pressure being higher than before (~day 4). We defined the pressure migration rate, which is the distance from the injection point (m)/elapsed time (h) and showed it in Figure 6. In this analysis, the events having pore pressure higher than wellhead pressure at its occurrence time are excepted. A correlation between the migration rate and pore pressure value has been confirmed. Time series change of average migration rate is shown in Figure 6. The migration rate of lower pore pressure was high, especially during the early stage of stimulation, but it decreased with the time or with an increasing number of moderate/higher pore pressure. Such phenomena were also studied through modeling (McClure and Horne, 2014), and they found that the difference of permeability of the fracture causes the different patterns of pore pressure migration. It is also necessary to consider the effect of advancing the stimulated zone front farther from the injection point, which produces greater flow resistance in proportion to the length of the flow path. After day 4, many of the events were induced by moderate/higher ΔP, indicating that fluid could also migrate into these fractures. However, eventually, the distribution process of the injected fluid into each fracture becomes increasingly complex.

CONCLUSION

We investigated the mechanism behind the large induced seismicity at the shut-in phase of hydraulic stimulation at Basel, Switzerland, to fully understand the physics behind the large induced seismicity. Also, we studied pore pressure migration during hydraulic stimulation at Basel to understand the physics of the reservoir creation process. We estimated pore pressure increase from the information of fault orientation and stress state. Then, we investigated the behavior of pore pressure migration during stimulation and after the shut-in phase. We also discussed the causality between the behavior of the shut-in pressure and the occurrence of large induced seismicity. At the shut-in phase, the seismic cloud still extended to the far-field, and large events preferentially occurred in this period. The hypocenters of these large events were located at the edge of the previously stimulated zone.

We found that lower pore pressure (~10 MPa, around 30% of the maximum injection pressure) migrated faster and farther. This phenomenon was explained as the consequence of a self-migration mechanism related to the high permeability of subcritical fractures. In contrast, moderate and higher pore pressure remained in the near field of the injection well until the wellhead pressure reached a certain level. After the start of the migration of medium pore pressure, the migration rate of lower pore pressure decreased significantly. This was interpreted to reflect an insufficient volume and pressure of fluid supplied to the edge of the permeable fracture. These insights suggest that there is an optimum wellhead pressure for each field, which would enable a more extensive and prolonged migration of a permeable fracture for more effective and economic reservoir creation.

Pore pressure migration progressed, even after shut-in, causing seismic events at the edge of the seismic cloud. Pore pressure increase at the periphery of the seismic cloud was sufficiently high to trigger induced seismicity. The pore pressure distributed uniformly at the edge region of the seismic cloud in several hours after shut-in. We interpreted that the change of pore pressure distribution

occurred even on the fault planes of large events that were situated at the edge of the seismic zone. This caused large parts of large existing faults to reach a critical state resulting in large events.

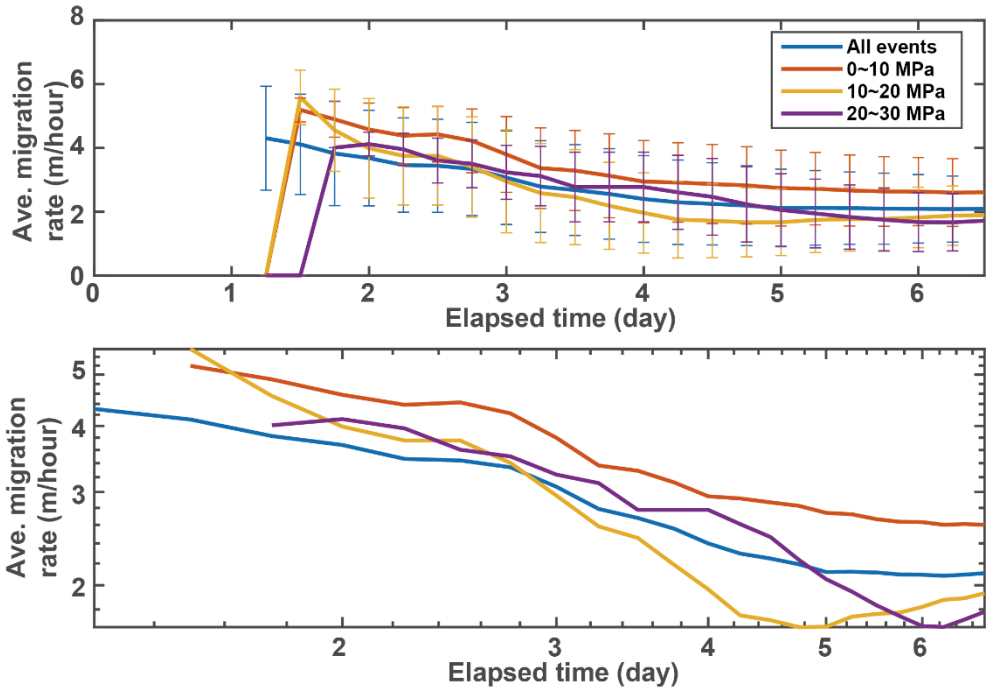

Figure 6. (Top) Average migration rate for lower, moderate, and higher ΔP, with an error bar of a standard deviation. (bottom) Averaging migration rate in a log-log scale.

ACKNOWLEDGEMENT

We thank Geo Explorers Ltd. and Geo- Energie Suisse AG for providing the microseismic wave data sets and for permission to publish the results. This study was supported by JSPS KAKENHI grant 13J09170/15 K20865, 16H04612, and Grant-in-Aid for JSPS Overseas Research Fellow. The microseismic data were proprietary of Geo Explorers Ltd. and Geo-Energie Suisse AG; not open to the public. Focal mechanism data and stress data are available in the literatures cited in this paper.

REFERENCES

Asanuma, H., Kumano, Y., Hotta, A., Niitsuma, H., Schanz, U., and Häring, M.: Analysis of microseismic events from a stimulation at Basel, Switzerland, *Geotherm. Resour. Counc. Trans*., **31**, (2007), 265–270.

Asanuma, H., Kumano, Y., Niitsuma, H., Schanz, U., and Häring, M.: Interpretation of reservoir structure from super-resolution mapping of microseismic multiplets from stimulation at Basel, Switzerland in 2006, *Geotherm. Resour. Counc. Trans*., **32**, (2008), 65–70.

Barton, C.A., Zoback, M.D., and Moos, D.: Fluid flow along potentially active faults in crystalline rock, *Geology*, **23**, (1995), 683–686.

Byerlee J.: Friction of rocks, *Pure Applied Geophysics*, **116(4-5)**, (2014), 615-626.

Catalli, F., Meier, M.A., and Wiemer, S.: The role of Coulomb stress changes for injection-induced seismicity: The Basel enhanced geothermal system, *Geophys. Res. Lett*., **40**, (2013), 72–77, doi:10.1029/2012GL054147.

Deichmann, N., Kraft, T., and Evans, K.F.: Identification of faults activated during the stimulation of the Basel geothermal project from cluster analysis and fault mechanisms for the larger magnitude events, *Geothermics*, **52**, (2014), 84–97, doi:10.1016/j.geothermics.2014.04.001.

Dinske, C., Shapiro, S. and Häring, M.: Interpretation of microseismicity induced by time-dependent injection pressure, *SEG Expanded Abstr*., **29**, (2010), 2125–2129, doi:10.1190/1.3513264.

Dyer, B.C., Schanz, U., Ladner, F., Häring, M.O., and Spillmann, T.: Microseismic imaging of a geothermal reservoir stimulation, *The Leading Edge*, **27**, (2008), 856–869, doi:10.1190/1.2954024.

Ellsworth, L. W. (2013), Injection-induced earthquake, Science, 341, doi:10.1126/science.1225942.

Evans, K. F., Moriya, H., Niitsuma, H., Jones, R.H., Phillips, W.S., Genter, A., Sausse, J., Jung, R., and Baria, R.: Microseismicity and permeability enhancement of hydrogeologic structures during massive fluid injections into granite at 3 km depth at the Soultz HDR site, *Geophys. J. Int*., **160(1)**, (2005), 389–412, doi:10.1111/j.1365-246X.2004.02474.x.

Häring, M. O., Schanz, U., Ladner, F., and Dyer, B.: Characterization of the Basel-1 enhanced geothermal system, *Geothermics*, **37**, (2008), 469–495, doi:10.1016/j.geothermics.2008.06.002.

Ito, T., and Zoback, M.D.: Fracture permeability and in situ stress to 7 km depth in the KTB scientific drillhole, *Geophys. Res. Lett.*, **27(7)**, (2000), 1045–1048.

Majer, E. L., Baria, R., Stark, M., Oates, S., Bommer, J., Smith, B., and Asanuma, H.: Induced seismicity associated with enhanced geothermal system, *Geothermics*, **36**, (2007), 185–222, doi:10.1016/j.geothermics.2007.03.003.

McClure, M., and Horne, R.: An investigation of stimulation mechanisms in enhanced geothermal systems, *Int. J. Rock Mech. Min. Sci*., **72**, (2014), 242–260.

Ghassemi, A., and Zhou, X.: A three-dimensional thermo-poroelastic model for fracture response to injection/extraction in enhanced geothermal systems, *Geothermics*, **40(1)**, (2011), 39–49.

Giardini, D.: Geothermal quake risks must be faced, *Nature*, **462(7275)**, (2009), 848–849, doi:10.1038/462848a.

Mukuhira,Y., Asanuma, H., Niitsuma, H., and Häring, M.: Characteristics of large-magnitude microseismic events recorded during and after stimulation of a geothermal reservoir at Basel, Switzerland, *Geothermics*, **45**, (2013), 1–7, doi:10.1016/ j.geothermics.2012.07.005.

Mukuhira, Y., Dinske, C., Asanuma, H., Ito, T., and Häring, M.O.: Pore pressure behavior at the shut-in phase and causality of large induced seismicity at Basel, Switzerland, *J. Geophys. Res. Solid Earth*, **121**, (2016), doi:10.1002/ 2016JB013338.

Mukuhira, Y., Moriya, H., Ito, T., Asanuma, H., and Häring, M.O.: Pore pressure migration during hydraulic stimulation due to permeability enhancement by low-pressure subcritical fracture slip, *Geophys. Res. Lett.*, **44**, (2017), doi:10.1002/2017GL072809.

Moriya, H., Niitsuma, H., and Baria, R.: Multiplet-clustering analysis reveals structural details within the seismic cloud at the Soultz geothermal field, France, *Bull. Seismol. Soc. Am*., **93(4)**, (2003), 1606–1620.

Segall, P., and Lu, S.: Injection-induced seismicity: Poroelastic and earthquake nucleation effects, J. *Geophys. Res. Solid Earth*, **120**, (2015), 5082–5103, doi:10.1002/2015JB012060.

Shapiro, S. A., and Dinske, C.: Fluid-induced seismicity: Pressure diffusion and hydraulic fracturing, *Geophys. Prospect*., **57**, (2009), 301–310.

Valley, B., and Evans, K.F.: Stress orientation to 5 km depth in the basement below Basel (Switzerland) from borehole failure analysis, *Swiss Journal of Geosciences*, **102**, (2009), 467–480.

Valley, B., and Evans, K.F.: Estimation of the stress magnitude in Basel enhanced geothermal system, *Proceedings WGC 2015*, (2015).

Waldhauser, F., and Ellsworth, W.L.: A double-difference earthquake location algorithm: Method and application to the Northern Hayward Fault, California, *Bull. Seismol. Soc. Am*., **90(6)**, (2000), 1353–1368.

Zoback, M.D., Reservoir Geomechanics. Cambridge University Press, (2007), New York, NY, USA, 449 p.